scientific reports

Check for updates

OPEN

Analytical technique and diverse chaos-identifying tools for the time fractional symmetric regularized long wave equation

Mohammad Safi Ullah, Md. Mehedi Hasan & Md. Aman Mahbub✉

The nonlinear conformable time-fractional symmetric regularized long wave (SRLW) equation is important in physics because it captures memory effects in fluid flow and describes how weakly nonlinear pulses evolve in optical fibers. This work solves the SRLW problem using the $\left(\frac{G'}{G^2}\right)$ -expansion technique and obtain diverse exact solutions, such as breather waves, kinky breathers, double kinks, local breathers with kink waves, local breathers with lump waves, and local breathers with dark-bright solitons. Then, the three-dimensional representations, along with their density plots for the real, imaginary, and absolute value parts of these solutions are displayed. We also detect the system's chaotic nature using various chaos-identifying tools, such as strange attractors, return maps, Lyapunov exponents, and others. The findings demonstrate the usefulness of the mentioned method as a mathematical tool for resolving nonlinear conformable time-fractional problems that arise in various mathematical fields.

Keywords Lyapunov exponents, -expansion method, Strange attractors, Chaotic analysis

Recently, nonlinear evolution equations have become a significant tool for modeling diverse real-life phenomena in the areas of contemporary science, including fluid dynamics[1], coastal engineering[2], nonlinear optics[3], plasma physics[4], and others. There have been multiple mathematical models introduced to explain these intricate systems, including the Yajima–Oikawa model[5], the Oskolkov Eq[6]., the Kudryashov-Sinelshchikov Eq[7]., the Jaulent–Miodek hierarchy Eq[8]., and many others. To discover the soliton dynamics and novel characteristics of these nonlinear problems, researchers have developed multiple techniques including the modified simple equation technique[9], the Wang's direct mapping method[10], ansatz approach[11], the extended auxiliary equation technique[12], $\tan\left(F\left(\frac{\xi}{2}\right)\right)$ -expansion method[13], modified generalized exponential rational function $_{\text{method}}$[14], the extension exponential rational function process[15], unified solver method[16], and many others.

Fractional calculus is at the forefront of ground-breaking research and is becoming increasingly widespread in various physical issues in nonlinear fields. Numerous researchers have also come up with fractional approaches, such as the Caputo-Fabrizio derivative[17], the modified Riemann-Liouville derivative[18], the local fractional derivative[19], the truncated M-fractional derivative[20], the conformable fractional derivative[21], and more.

The conformable fractional derivative is a forthright definition of the fractional derivative. A conformable fractional derivative is less complex than using a fractional derivative. The conformable fractional derivative obeys certain standard principles that other fractional derivatives do not satisfy, including the chain rule. The sole limitation is that the conformable fractional derivative of every differentiable function at zero is equal to zero. To overcome this problem, a suitable fractional derivative is suggested in[22,23].

In this work, we utilize $\left(\frac{G'}{G^2}\right)$ -expansion technique[24] to derive the exact solutions of the conformable time-fractional nonlinear SRLW problem. This research also uses strange attractors, recurrence plots, return maps, Lyapunov exponents, power spectrum plots, 3D and 2D phase diagrams, and fractal dimensions to identify and inspect the chaos of this nonlinear problem. To the best of the author's knowledge, there has never been an investigation into the relationship between these types of studies and the analysis of this nonlinear model.

We consider the following SRLW model, which arises in nonlinear fluid waves[25,26],

Department of Mathematics, Comilla University, Cumilla 3506, Bangladesh. ✉email: rinko.math@cou.ac.bd

$$D_{tt}^{2\beta}\, p + up_{xx} + vpD_t^{\beta}\, p_x + vp_x D_t^{\beta}\, p + wD_{tt}^{2\beta}\, p_{xx} = 0,\ \ t > 0 \tag{1}$$

where $p = p(x, t)$ is the amplitude portion of solitons, u, v and w real parameters, $D_{tt}^{2\beta}$ is the differential operator with fractions of order 2β in conformable perception. With its modest nonlinearity, this equation offers an intriguing model for electrostatics and charge density fluctuations.

This article is structured into 12 sections, where Sect. 1 contains the introduction with the graphical abstract (see Fig. 1) of this work. Section 2 describes the conformable fractional derivatives. Section 3 contains the $\left(\frac{G'}{G^2}\right)$ expansion algorithm, and Sect. 4 comprises its applications. Section 5 provides the graphical representations of the solutions. Section 6 corresponds to the stability analysis of the obtained solution. Section 7 delivers the chaotic analysis by Lyapunov exponents and other tools. Section 8 includes multi-stability analysis. Section 9 explains the uniqueness of our approach and the obtained results. Section 10 covers the future-oriented studies. Finally, Sect. 11 is for the conclusion.

The conformable fractional derivative's preface

This section presents fundamental definitions and theorems relevant to the conformable fractional derivative. The conformable derivative[27] of order β, for the independent variable t, is defined as follows:

$$D_t^{\beta}\ (p(t)) = \lim_{h \to 0} \frac{p\left(t + ht^{1-\beta}\right) - p(t)}{h},\quad t > 0,\ \ \beta \in (0,1]$$

where the function $p = p(t)\ : [0, \infty) \to \mathbb{R}$ exist.

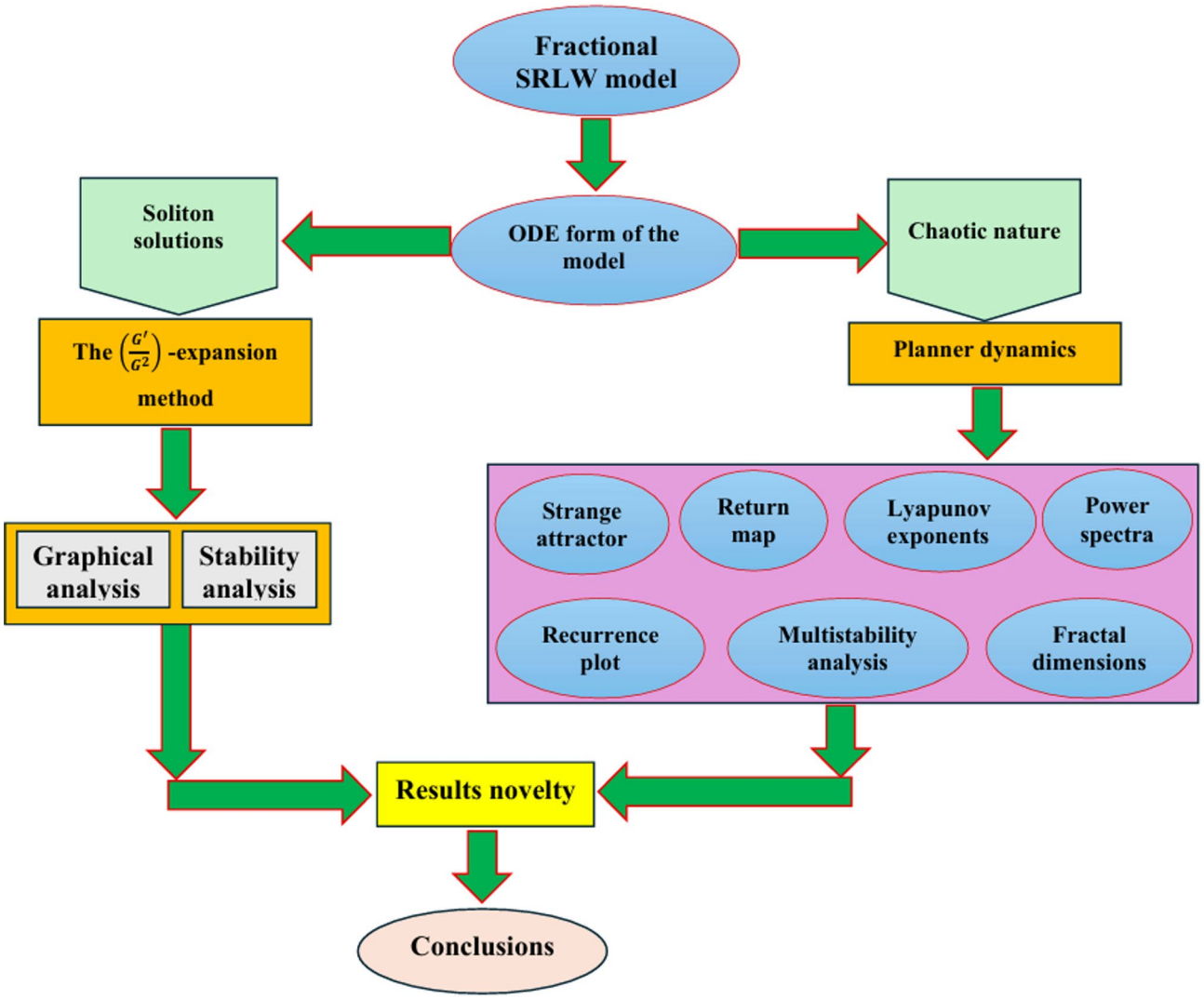


Fig. 1. Graphical abstract.

Theorem 2.1 [28] Suppose that the derivative's order $\beta \in (0,1]$ and let us say, $p = p(t)$ and $\mu = \mu(t)$ are β -differentiable for all non-negative t. Then,

1. $D_t^\beta (c_1 p + c_2 \mu) = c_1 D_t^\beta (p) + c_2 D_t^\beta (\mu), \ \forall \ c_1, c_2 \in \mathbb{R}.$
2. $D_t^\beta \left(t^l\right) = l t^{l-\beta}, \ \forall \ l \in \mathbb{R}.$
3. $D_t^\beta (\lambda) = 0, \forall$ constant function $p(t) = \lambda$ ..
4. $D_t^\beta (p\mu) = p D_t^\beta (\mu) + \mu D_t^\beta (p)$.
5. $D_t^\beta \left(\frac{p}{\mu}\right) = \frac{\mu D_t^\beta (\mu p) - p D_t^\beta (\mu)}{\mu^2}$.
6. $D_t^\beta (p)(t) = t^{1-\beta} \frac{dp}{dt}$.

Theorem 2.2 [29] Let $p = p(t)$ be a function, which is differentiable and β -conforming, and suppose that μ is defined and differentiable within the range of p.Then,

$$D_t^a (p \, o \, \mu)(t) = t^{1-\beta} \mu'(t) p\prime (\mu(t))$$

Certain essential fundamental features, such as the Laplace transform, Taylor series expansion, and chain rule, are satisfied by conformable fractional differential[30] operators.

The $\left(\frac{G'}{G^2}\right)$-expansion algorithm

Within this section, we describe the $\left(\frac{G'}{G^2}\right)$ -expansion technique that is covered in[31,32]. With independent variables, x and t, examine the successive partial differential equations for nonlinear evolution:

$$L(p, p_t, p_x, p_{tt}, p_{xx}, p_{xt}, \ldots) = 0 \tag{2}$$

where L is a polynomial in p, incorporating numerous partial derivatives, employing nonlinear elements and the higher-order derivatives, and $p(x,t)$ is an unidentified function of the independent variables x, t. The fundamental processes for obtaining exact solutions to NPDEs are as follows.

Step 1 Employ the traveling wave transformation in a variable γ to turn a nonlinear partial differential equation (PDE) in (2) into an ordinary differential equation (ODE) as outlined below.

$$p(x,t) = P(\gamma), \ \gamma = a\left(x - q\frac{t^\beta}{\beta}\right) \tag{3}$$

where the arbitrary constants a and q are nonzero. It should be declared that for some specific problems, another transform, $\gamma = a\left(x - q\frac{t^\beta}{\beta}\right)$, may rarely be applied. Using as many integrations for γ as possible, and the transformation in (3) and (2) is converted to an ODE in $P = P(\gamma)$ as follows:

$$Q\left(P, P', P'', P''', \ldots\right) = 0 \tag{4}$$

A polynomial of $P(\gamma)$ and its different derivatives are denoted by Q. The derivative for γ, is shown by the prime notation (').

Step 2 Assume that the powers of $\left(\frac{G'}{G^2}\right)$ can be used to represent the constitutional solution of the ODE in (4) as follows.

$$P(\gamma) = l_0 + \sum_{i=1}^{K} \left[l_i \left(\frac{G\prime}{G^2}\right)^i + l_{-i} \left(\frac{G\prime}{G^2}\right)^{-i} \right] \tag{5}$$

where the following nonlinear ODE is satisfied by $G = G(\gamma)$:

$$\left(\frac{G\prime}{G^2}\right)' = \alpha + A\left(\frac{G\prime}{G^2}\right)^2 \tag{6}$$

where A and α are both arbitrary constants. It is not possible for both unknown constants, l_K and l_{-K}, to be zero at the same time. The coefficients l_0, l_i, l_{-i} $(i = 1,2, \ldots, K)$ are unknown constants that will be discovered in a subsequent phase.

Step 3 By applying the homogeneous balance principle, which involves striking a balance between the nonlinear factors in (4) and the highest order derivatives, the value of the positive integer K can be obtained. More specifically, the degree of the other terms will be represented as follows if the degree of $P(\gamma)$ is deg $P(\gamma) = K$,

$$deg\left[\frac{d^r P(\gamma)}{d\gamma^r}\right] = K + r,\ deg\left[(P(\gamma))^p\left(\frac{d^r P(\gamma)}{d\gamma^r}\right)^m\right] = Kp + m(K + r) \tag{7}$$

Step 4 We find a polynomial in $\left(G\prime/G^2\right)$ by substituting (5) and (6) into (4). We develop a set of algebraic equations for the unknown constants. By gathering all coefficients of similar power of $\left(G\prime/G^2\right)$ and set all the collected coefficients to zero. Assume that symbolic software applications such as Maple can be utilized to resolve the resultant algebraic equations for the unknown constants.

Step 5 The three cases listed below can be used to group the general solutions of (6), in which f and g are arbitrary constants, where $f, g \neq 0$..

$A\alpha > 0$, after that, we obtain the general solution

$$\frac{G\prime}{G^2} = \sqrt{\frac{\alpha}{A}}\left(\frac{f\,cos\left(\sqrt{A\alpha}\,\gamma\right) + g\sin\left(\sqrt{A\alpha}\,\gamma\right)}{g\,cos\left(\sqrt{A\alpha}\,\gamma\right) - f\sin\left(\sqrt{A\alpha}\,\gamma\right)}\right) \tag{8}$$

$A\alpha < 0$, then we obtain the general solution

$$\frac{G\prime}{G^2} = -\frac{\sqrt{|A\alpha|}}{A}\left(\frac{f\,sinh\left(2\sqrt{|A\alpha|}\gamma\right) + f\cosh\left(2\sqrt{|A\alpha|}\gamma + g\right)}{f\,sinh\left(2\sqrt{|A\alpha|}\gamma\right) + f\cosh\left(2\sqrt{|A\alpha|}\gamma - g\right)}\right) \tag{9}$$

If $A \neq 0$ and $\alpha = 0$, then we obtain the general solution

$$\frac{G\prime}{G^2} = -\frac{f}{A(f\gamma + g)} \tag{10}$$

The exact and explicit solutions of (2) can be acquired by putting the value of unknowns and the solutions in (8) − (10) into (5) with the transformation in (3).

Application of $\left(\frac{G\prime}{G^2}\right)$ algorithm

Consider the wave transform that follows:

$$p(x,t) = P(\gamma),\ \gamma = a\left(x - q\frac{t^\beta}{\beta}\right) \tag{11}$$

where q and a are the wave velocity and the wave height, respectively.

By substituting (11) into (1) and integrating once for γ. Then, for additional computation, let us assume that the arbitrary constant to 0. we obtain a nonlinear ordinary differential Eq.

$$\left(q^2 + u\right)P + wq^2a^2P'' - vq\frac{P^2}{2} = 0 \tag{12}$$

for which the principle of homogeneous balancing is used. By following Step 3 of the previously described procedure. The second-order derivative $P\prime\prime$ and the nonlinear term of the highest order P^2 are equalized using formula (7) as follows:

$$deg\left[P\prime\prime\right] = K + 2 = deg\left[P^2\right] = Kp + 2(K + 0) \tag{13}$$

which leads to $K = 2$. Therefore, using the $\left(\frac{G\prime}{G^2}\right)$ expansion method, we find the exact solutions of the ODE in (12) that can be written as,

$$P(\gamma) = l_0 + l_1\left(\frac{G\prime}{G^2}\right) + l_{-1}\left(\frac{G\prime}{G^2}\right)^{-1} + l_2\left(\frac{G\prime}{G^2}\right)^2 + l_{-2}\left(\frac{G\prime}{G^2}\right)^{-2} \tag{14}$$

where l_0, l_1, l_{-1}, l_2, and l_{-2} are unknown constants. Take the place of (14) into (12) along with (6), then compile every coefficient with a similar power of $\left(\frac{G\prime}{G^2}\right)$, and then, these resultant coefficients are set to zero. Consequently, we derive the subsequent algebraic equations:

$$\begin{cases} 6wq^2a^2l_2\alpha^{\,2} - \frac{1}{2}vql_2^2 = 0, \\ 2a^2\alpha^{\,2}q^2wl_1 - qvl_1l_2 = 0, \\ -\frac{1}{2}vql_1^2 - vql_2l_0 + l_2u + l_2q^2 + 8wq^2a^2l_2\alpha\, A = 0, \\ 2Aa^2\alpha\, q^2wl_1 - qvl_{-1}l_2 - qvl_0l_1 + q^2l_1 + ul_1 = 0, \\ -\frac{1}{2}vql_0^2 + l_0q^2 + l_0u + 2wq^2a^2l_2A^2 + 2wq^2a^2l_{-2}\alpha^{\,2} - vql_2l_{-2} - vql_1l_{-1} = 0 \\ 2Aa^2\alpha\, q^2wl_{-1} - qvl_{-2}l_1 - qvl_{-1}l_0 + q^2l_{-1} + ul_{-1} = 0, \\ -\frac{1}{2}vql_{-1}^2 - vql_0l_{-2} + l_{-2}q^2 + l_{-2}u + 8wq^2a^2l_{-2}\alpha\, A = 0, \\ 2A^2a^2q^2wl_{-1} - qvl_{-2}l_{-1} = 0, \\ 6A^2a^2q^2wl_{-2} - \frac{1}{2}qvl_{-2}^2 = 0. \end{cases} \tag{15}$$

We find the following six solution sets when we use Maple to solve the obtained algebraic system (15).

Case 1
$$A = -\frac{q^2+u}{4a^2\alpha\, q^2w},\ \alpha\ = \alpha\ ,\ l_{-2} = 0,\ l_{-1} = 0,\ l_0 = -\frac{q^2+u}{vq},\ l_1 = 0,\ l_2 = \frac{12wqa^2\alpha^{\,2}}{v} \tag{16}$$

Case 2
$$A = \frac{q^2+u}{4a^2\alpha\, q^2w},\ \alpha\ = \alpha\ ,\ l_{-2} = 0,\ l_{-1} = 0,\ l_0 = -\frac{3\left(q^2+u\right)}{vq},\ l_1 = 0,\ l_2 = \frac{12wqa^2\alpha^{\,2}}{v} \tag{17}$$

Case 3
$$A = A,\ \alpha\ = -\frac{q^2+u}{4Aa^2q^2w},\ l_{-2} = \frac{12wqa^2A^2}{v},\ l_{-1} = 0,\ l_0 = -\frac{q^2+u}{vq},\ l_1 = 0,\ l_2 = 0 \tag{18}$$

Case 4
$$A = A,\ \alpha\ = \frac{q^2+u}{4Aa^2q^2w},\ l_{-2} = \frac{12wqa^2A^2}{v}\ ,\ \ l_{-1} = 0,\ l_0 = \frac{3\left(q^2+u\right)}{vq},\ l_1 = 0,\ l_2 = 0 \tag{19}$$

Case 5
$$l_{-1} = 0, l_0 = \frac{q^2+u}{2vq},\ l_1 = 0,\ l_2 = \frac{3(q^4+2q^2u+u^2)}{64A^2a^2q^3vw} \tag{20}$$

Case 6
$$A = A,\ \alpha\ = -\frac{q^2+u}{16Aa^2q^2w},\ l_{-2} = \frac{12wqa^2A^2}{v}$$
$$l_0 = \frac{3}{2}\frac{q^2+u}{vq},\ l_1 = 0,\ l_2 = \frac{3(q^4+2q^2u+u^2)}{64A^2a^2q^3vw}$$
$$A = A,\ \alpha\ = \frac{q^2+u}{16Aa^2q^2w},\ l_{-2} = \frac{12wqa^2A^2}{v}\ ,\ l_{-1} = 0 \tag{21}$$

For case 1 Using (8) − (10) with (11), (14), and (16), we obtain the following solutions for (1).

When $A\alpha\ > 0$, the trigonometric solution can be obtained as follows

$$p_{11}\left(x,t\right) = l_0 + l_2\left(\sqrt{\frac{\alpha}{A}}\left(\frac{f\ cos\left(\sqrt{A\alpha}\,\gamma\right) + g\sin\left(\sqrt{A\alpha}\,\gamma\right)}{g\ cos\left(\sqrt{A\alpha}\,\gamma\right) - f\sin\left(\sqrt{A\alpha}\,\gamma\right)}\right)\right)^2$$

when $A\alpha\ < 0$, the hyperbolic solution can be obtained as follows,

$$p_{12}\left(x,t\right) = l_0 + l_2\left(-\frac{\sqrt{|A\alpha\,|}}{A}\left(\frac{f\ sinh\left(2\sqrt{|A\alpha\,|}\gamma\right) + f\cosh\left(2\sqrt{|A\alpha\,|}\gamma\ + g\right)}{f\ sinh\left(2\sqrt{|A\alpha\,|}\gamma\right) + f\cosh\left(2\sqrt{|A\alpha\,|}\gamma\ - g\right)}\right)\right)^2$$

$$\text{where } A = -\frac{1}{4}\frac{q^2+u}{a^2\alpha\, q^2w},\ l_0 = -\frac{q^2+u}{vq},\ l_2 = \frac{12wqa^2\alpha^{\,2}}{v},\ \gamma\ = a\left(x - q\frac{t^\beta}{\beta}\right)$$

For case 2 Using (8) − (10) with (11), (14), and (17), we obtain the following solutions for (1).

When $A\alpha\ > 0$, the trigonometric solution can be obtained as follows

$$p_{21}\left(x,t\right) = l_0 + l_2\left(\sqrt{\frac{\alpha}{A}}\left(\frac{f\ cos\left(\sqrt{A\alpha}\,\gamma\right) + g\sin\left(\sqrt{A\alpha}\,\gamma\right)}{g\ cos\left(\sqrt{A\alpha}\,\gamma\right) - f\sin\left(\sqrt{A\alpha}\,\gamma\right)}\right)\right)^2$$

when $A\alpha\ < 0$, the hyperbolic solution can be obtained as follows

$$p_{22}(x,t) = l_0 + l_2\left(-\frac{\sqrt{|A\alpha|}}{A}\left(\frac{f\,sinh\left(2\sqrt{|A\alpha|}\gamma\right) + f\cosh\left(2\sqrt{|A\alpha|}\gamma + g\right)}{f\,sinh\left(2\sqrt{|A\alpha|}\gamma\right) + f\cosh\left(2\sqrt{|A\alpha|}\gamma - g\right)}\right)\right)^2$$

$$\text{where } A = \frac{1}{4}\frac{q^2+u}{a^2\alpha\, q^2 w},\ l_0 = -\frac{3\left(q^2+u\right)}{vq},\ l_2 = \frac{12wqa^2\alpha^2}{v},\ \gamma = a\left(x - q\frac{t^\beta}{\beta}\right)$$

For case 3 Using (8) − (10) with (11), (14), and (18), we obtain the following solutions for (1).

When $A\alpha > 0$, the trigonometric solution can be obtained as follows

$$p_{31}(x,t) = l_0 + l_{-2}\left(\sqrt{\frac{\alpha}{A}}\left(\frac{f\,cos\left(\sqrt{A\alpha}\,\gamma\right) + g\sin\left(\sqrt{A\alpha}\,\gamma\right)}{g\,cos\left(\sqrt{A\alpha}\,\gamma\right) - f\sin\left(\sqrt{A\alpha}\,\gamma\right)}\right)\right)^{-2}$$

when $A\alpha < 0$, the hyperbolic solution can be obtained as follows,

$$p_{32}(x,t) = l_0 + l_{-2}\left(-\frac{\sqrt{|A\alpha|}}{A}\left(\frac{f\,sinh\left(2\sqrt{|A\alpha|}\gamma\right) + f\cosh\left(2\sqrt{|A\alpha|}\gamma + g\right)}{f\,sinh\left(2\sqrt{|A\alpha|}\gamma\right) + f\cosh\left(2\sqrt{|A\alpha|}\gamma - g\right)}\right)\right)^{-2}$$

when $A \neq 0$ and $\alpha = 0$, the trigonometric solution can be obtained as follows

$$p_{33}(x,t) = l_0 + l_{-2}\left(-\frac{f}{A(f\gamma + g)}\right)^{-2}$$

$$\text{where } \alpha = -\frac{1}{4}\frac{q^2+u}{Aa^2q^2w},\ l_0 = -\frac{q^2+u}{vq},\ l_{-2} = \frac{12wqa^2A^2}{v},\ \gamma = a\left(x - q\frac{t^\beta}{\beta}\right)$$

For case 4 Using (8) − (10) with (11), (14), and (19), we obtain the following solutions for (1).

When $A\alpha > 0$, the trigonometric solution can be determined as follows

$$p_{41}(x,t) = l_0 + l_{-2}\left(\sqrt{\frac{\alpha}{A}}\left(\frac{f\,cos\left(\sqrt{A\alpha}\,\gamma\right) + g\sin\left(\sqrt{A\alpha}\,\gamma\right)}{g\,cos\left(\sqrt{A\alpha}\,\gamma\right) - f\sin\left(\sqrt{A\alpha}\,\gamma\right)}\right)\right)^{-2}$$

when $A\alpha < 0$, the hyperbolic solution can be determined as follows

$$p_{42}(x,t) = l_0 + l_{-2}\left(-\frac{\sqrt{|A\alpha|}}{A}\left(\frac{f\,sinh\left(2\sqrt{|A\alpha|}\gamma\right) + f\cosh\left(2\sqrt{|A\alpha|}\gamma + g\right)}{f\,sinh\left(2\sqrt{|A\alpha|}\gamma\right) + f\cosh\left(2\sqrt{|A\alpha|}\gamma - g\right)}\right)\right)^{-2}$$

when $A \neq 0$ and $\alpha = 0$, the trigonometric solution can be determined as follows

$$p_{43}(x,t) = l_0 + l_{-2}\left(-\frac{f}{A(f\gamma + g)}\right)^{-2}$$

$$\text{where } \alpha = \frac{1}{4}\frac{q^2+u}{Aa^2q^2w},\ l_0 = \frac{3\left(q^2+u\right)}{vq},\ l_{-2} = \frac{12wqa^2A^2}{v},\ \gamma = a\left(x - q\frac{t^\beta}{\beta}\right)$$

For case 5 Using (8) − (10) with (11), (14), and (20), we obtain the following solutions for (1).

When $A\alpha > 0$, the trigonometric solution can be determined as follows

$$p_{51}(x,t) = l_0 + l_2\left(\sqrt{\frac{\alpha}{A}}\left(\frac{f\,cos\left(\sqrt{A\alpha}\,\gamma\right) + g\sin\left(\sqrt{A\alpha}\,\gamma\right)}{g\,cos\left(\sqrt{A\alpha}\,\gamma\right) - f\sin\left(\sqrt{A\alpha}\,\gamma\right)}\right)\right)^{2} + l_{-2}\left(\sqrt{\frac{\alpha}{A}}\left(\frac{f\,cos\left(\sqrt{A\alpha}\,\gamma\right) + g\sin\left(\sqrt{A\alpha}\,\gamma\right)}{g\,cos\left(\sqrt{A\alpha}\,\gamma\right) - f\sin\left(\sqrt{A\alpha}\,\gamma\right)}\right)\right)^{-2}$$

when $A\alpha < 0$, the hyperbolic solution can be obtained as follows

$$p_{52}(x,t) = l_0 + l_2\left(-\frac{\sqrt{|A\alpha|}}{A}\left(\frac{f\,sinh\left(2\sqrt{|A\alpha|}\gamma\right) + f\cosh\left(2\sqrt{|A\alpha|}\gamma + g\right)}{f\,sinh\left(2\sqrt{|A\alpha|}\gamma\right) + f\cosh\left(2\sqrt{|A\alpha|}\gamma - g\right)}\right)\right)^2$$
$$+l_{-2}\left(-\frac{\sqrt{|A\alpha|}}{A}\left(\frac{f\,sinh\left(2\sqrt{|A\alpha|}\gamma\right) + f\cosh\left(2\sqrt{|A\alpha|}\gamma + g\right)}{f\,sinh\left(2\sqrt{|A\alpha|}\gamma\right) + f\cosh\left(2\sqrt{|A\alpha|}\gamma - g\right)}\right)\right)^{-2}$$

when $A \neq 0$ and $\alpha = 0$, the trigonometric solution can be obtained as follows

$$p_{53}(x,t) = l_0 + l_2\left(-\frac{f}{A(f\varsigma + g)}\right)^2 + l_{-2}\left(-\frac{f}{A(f\varsigma + g)}\right)^{-2}$$

where $\alpha = -\frac{1}{16}\frac{q^2+u}{Aa^2q^2w}$, $l_0 = \frac{1}{2}\frac{q^2+u}{vq}$, $l_{-2} = \frac{12wqa^2A^2}{v}$, $l_2 = \frac{3}{64}\frac{q^4+2q^2u+u^2}{A^2a^2q^3vw}$, $\gamma = a\left(x - q\frac{t^\beta}{\beta}\right)$.

For case 6 Using (8) $-$ (10) with (11), (14), and (21), we obtain the following solutions for (1).

When $A\alpha > 0$, the trigonometric solution can be obtained as follows

$$p_{61}(x,t) = l_0 + l_2\left(\sqrt{\frac{\alpha}{A}}\left(\frac{f\,cos\left(\sqrt{A\alpha}\gamma\right) + g\sin\left(\sqrt{A\alpha}\gamma\right)}{g\,cos\left(\sqrt{A\alpha}\gamma\right) - f\sin\left(\sqrt{A\alpha}\gamma\right)}\right)\right)^2 + l_{-2}\left(\sqrt{\frac{\alpha}{A}}\left(\frac{f\,cos\left(\sqrt{A\alpha}\gamma\right) + g\sin\left(\sqrt{A\alpha}\gamma\right)}{g\,cos\left(\sqrt{A\alpha}\gamma\right) - f\sin\left(\sqrt{A\alpha}\gamma\right)}\right)\right)^{-2}$$

when $A\alpha < 0$, the hyperbolic solution can be obtained as follows

$$p_{62}(x,t) = l_0 + l_2\left(-\frac{\sqrt{|A\alpha|}}{A}\left(\frac{f\,sinh\left(2\sqrt{|A\alpha|}\gamma\right) + f\cosh\left(2\sqrt{|A\alpha|}\gamma + g\right)}{f\,sinh\left(2\sqrt{|A\alpha|}\gamma\right) + f\cosh\left(2\sqrt{|A\alpha|}\gamma - g\right)}\right)\right)^2$$
$$+l_{-2}\left(-\frac{\sqrt{|A\alpha|}}{A}\left(\frac{f\,sinh\left(2\sqrt{|A\alpha|}\gamma\right) + f\cosh\left(2\sqrt{|A\alpha|}\gamma + g\right)}{f\,sinh\left(2\sqrt{|A\alpha|}\gamma\right) + f\cosh\left(2\sqrt{|A\alpha|}\gamma - g\right)}\right)\right)^{-2}$$

when $A \neq 0$ and $\alpha = 0$, the trigonometric solution can be as follows

$$p_{63}(x,t) = l_0 + l_2\left(-\frac{f}{A(f\gamma + g)}\right)^2 + l_{-2}\left(-\frac{f}{A(f\gamma + g)}\right)^{-2}$$

where $\alpha = \frac{1}{16}\frac{q^2+u}{Aa^2q^2w}$, $l_0 = \frac{3}{2}\frac{q^2+u}{vq}$, $l_{-2} = \frac{12wqa^2A^2}{v}$, $l_2 = \frac{3}{64}\frac{q^4+2q^2u+u^2}{A^2a^2q^3vw}$, $\gamma = a\left(x - q\frac{t^\beta}{\beta}\right)$.

Graphical representation

Figure 2 illustrates that $Re(p_{11})$ displays local breathers with a kink wave, while $Im(p_{11})$ displays breather wave, and $|p_{11}|$ denotes local breathers with dark soliton, using the values $\alpha = 1$, $q = 1$, $u = 1, a = 2$, $w = -1, v = 2.5, \beta = 0.5$, $f = 1$, and $g = 1$. Additionally, the patterns are the same for p_{21}, p_{31}, p_{41}, p_{43}, p_{51}, p_{53}, p_{61}, and p_{63}.

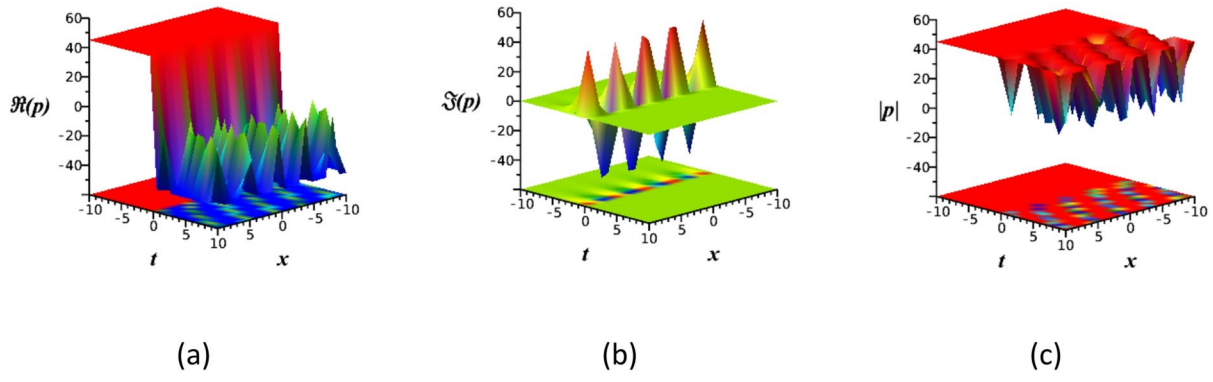
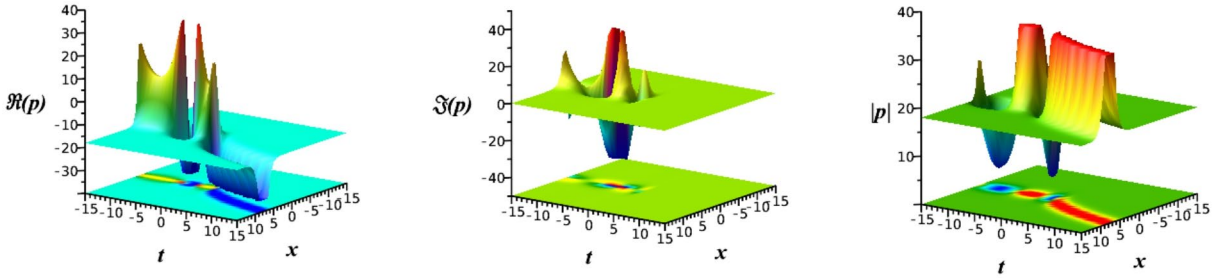
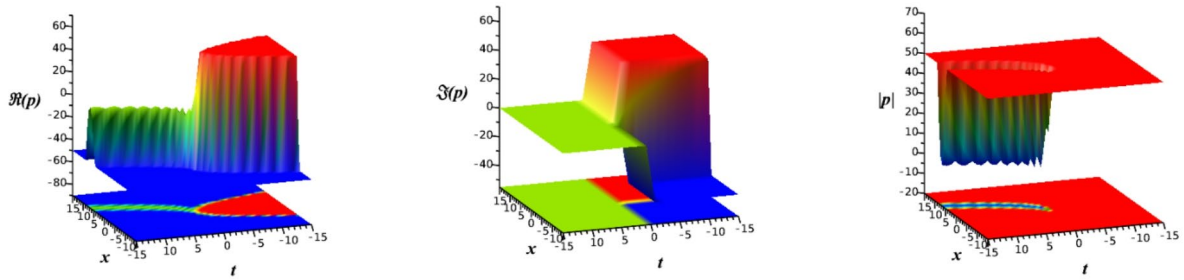


Fig. 2. Representation of $p_{11}(x,t)$ for the values $\alpha = 1$, $q = 1$, $u = 1, a = 2$, $w = -1, v = 2.5$, $\beta = 0.5$, $f = 1$, and $g = 1$.



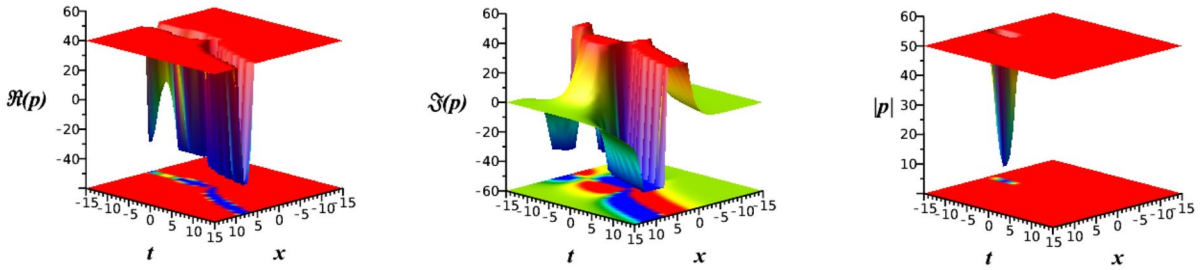
(a) (b) (c)

Fig. 3. Representation of $p_{22}(x,t)$ for the values $\alpha = 1,\ q = 1,\ u = 1,\ a = 1,\ w = -1$,.



(a) (b) (c)

Fig. 4. Representation of $p_{33}(x,t)$ for the values $\alpha = 0,\ q = 1,\ u = -1,\ a = 1,\ w = -1,\ v = 1,\ \beta = 0.5,\ f = 1$, and $g = 1$.



(a) (b) (c)

Fig. 5. Representation of $p_{52}(x,t)$ for the values $\alpha = 1,\ q = 1,\ u = 1,\ a = 1,\ w = 4,\ v = 1,\ \beta = 0.5,\ f = 1$, and $g = 1$.

$$v = 1,\ \beta = 0.5,\ f = 1,\ \text{and}\ g = 1$$

Figure 3 displays local breathers with lump waves. Using the values $\alpha = 1,\ q = 1,\ u = 1,\ a = 1,\ w = -1,\ v = 1,\ \beta = 0.5,\ f = 1$, and $g = 1$. Additionally, the patterns are the same for p_{12}.

Figure 4 illustrates that $Re\,(p_{33})$ displays kinky breathers, while $Im\,(p_{33})$ and $|p_{33}|$ display double kink and local breather wave, respectively, using the values $\alpha = 0,\ q = 1,\ u = -1,\ a = 1,\ w = -1,\ v = 1,\ \beta = 0.5,\ f = 1$, and $g = 1$. Additionally, the patterns are the same for p_{32}, p_{42}, p_{52}, and p_{62}.

Figure 5 illustrates that $Re\,(p_{52})$ displays a local breather with a dark soliton, while $Im\,(p_{52})$ and $|p_{52}|$ displays local breather with dark & bright soliton and breather wave, respectively, using the values $\alpha = 1,\ q = 1,\ u = 1,\ a = 1,\ w = 4,\ v = 1,\ \beta = 0.5,\ f = 1$, and $g = 1$. Additionally, the patterns are the same for p_{32}, p_{42}, p_{52}, and p_{62}.

1. Considering the following function: $L_{i+1} = \xi(L_i)$, where L_i corresponds to the state with the iteration i, and ξ represents the system function.
2. Select a point that is close to the primary assumption of the trajectory $L_i(\varphi_0)$.
3. Let $L_i + \delta L_i$ is the neighboring point with a tiny disturbance δL_i.
4. Supported by the Taylor theorem for the disturbance $\delta L_{i+1} = \frac{d\xi}{dL_i}\delta L_i + \cdots$, where $\frac{d\xi}{dL_i}$ is the Jacobian of ξ for L_i.
5. Consider $e^{\varrho} = \left|\frac{\delta L_{i+1}}{\delta L_i}\right| = \left|\frac{d\xi}{dL_i}\right|$, where ϱ is the local Lyapunov exponent.
6. $\varrho_i = \ln\left|\frac{d\xi}{dL_i}\right|$ is the local Lyapunov exponent with the iteration i.
7. The following global Lyapunov exponent can be obtained by averaging over n iterations: $\varrho = \lim_{n\to 0}\frac{1}{n}\sum_{i=0}^{n-1}\ln\left|\frac{d\xi}{dL_i}\right|$.

Algorithm of Lyapunov exponent computation.

Stability analysis of the solution

The stability properties[33,34] of the conformable time-fractional symmetric regularized long wave (SRLW) equation's solution are investigated below. To reach our destination, assume the Hamiltonian factor employing Eq. (1) as

$$S(q) = \frac{1}{2}\int_{-\infty}^{\infty}\frac{p(x,t)^2}{2}dx \tag{22}$$

Now, the sufficient condition for this solution's stability is as follows:

$$\frac{\partial S(q)}{\partial q} > 0 \tag{23}$$

where q is the wave velocity component. Finding stability for the solution P_{41} and taking the limit $x \in [-3,3]$ in Eq. (22). Then this reaches,

$$S(q) = \frac{9q}{2v} + \frac{9u}{2vq} + \frac{24a^4A^4wq^3\left(-3 + \frac{2a\left(f^2+g^2\right)wq\sin\left(\frac{3\sqrt{q^2+u}}{2awq}\right)}{f\sqrt{q^2+u}\left(f\cos\left(\frac{3\sqrt{q^2+u}}{2awq}\right)+g\sin\left(\frac{3}{2}\sqrt{\frac{q^2+u}{a^2wq^2}}\right)\right)}\right)}{(q^2+u)v} \tag{24}$$

In Eq. (24), using the stability requirement Eq. (23) and the assumption $u = a = v = f = g = 1$, $w = -1$, and $A = 0.5$ yields the stability condition of the solution P_{41} as follows:

$$\frac{\partial S(q)}{\partial q} = \frac{9q}{2} + \frac{9}{2q} + \frac{1.5q^3\left(-3 + \frac{4q\sin\left(\frac{3\sqrt{q^2+1}}{2q}\right)}{\sqrt{q^2+1}\left(\cos\left(\frac{3\sqrt{q^2+1}}{2q}\right)+\sin\left(\frac{3}{2}\sqrt{\frac{q^2+1}{q^2}}\right)\right)}\right)}{(q^2+1)} > 0 \tag{25}$$

Consequently, we get $\frac{\partial S(q)}{\partial q}\Big|_{q=0.3} = 16.36518889$ which is positive. For the condition Eq. (25), P_{41} is a stable solution. The same method can be used to determine the stability condition of other outcomes.

Chaotic analysis by lyapunov exponents and other tools

Chaos is the term used to describe situations in which some vibrant structures act in a manner that appears random but is controlled by deterministic rules[35]. Minor alterations to the initial values can lead to significantly divergent long-term results due to the great sensitivity of chaotic systems to early conditions. Chaos can emerge in various anthropogenic and natural systems, such as fluid dynamics, atmospheric circulation, and optics[36,37]. This section explores the chaotic behaviors of the solutions arrived at in the above problem. This inquiry includes

an analysis of both 2D and 3D phase representations. Let the dynamic system be obtained from Eq. (11) by setting $\frac{dP}{d\gamma} = Q$, then

$$\frac{dP}{d\gamma} = Q,\ \frac{dQ}{d\gamma} = -\alpha_1 P^2 - \alpha_2 P + Asin(\phi\gamma) \tag{26}$$

where $\alpha_1 = -\frac{vq}{2wq^2a^2}$ and $\alpha_2 = \frac{q^2+u}{wq^2a^2}$ with $wq^2a^2 \neq 0$. The external force is represented by $Asin(\phi\gamma)$, in Eq. (26) of the system discussed above, where ϕ and A signify the strength and rate of recurrence of the disturbance, respectively.

An effective method for determining the stability and chaos of dynamical systems[38,39] is the Lyapunov exponent, which is visualized mathematically. However, understanding system dynamics and utilizing well-organized data are crucial. The Lyapunov exponent is a crucial tool for finding whether a system is chaotic. If the exponent is large and the adjacent trajectories display exponential divergence, signifying chaotic behavior, if it is negative, the close trajectories give exponential convergence and indicate stability. The computation of such an exponential is necessary to understand nonlinear dynamics. We now determine that the Lyapunov exponents for the system (26) are $LE_1 = 1.0747$, $LE_2 = -1.2072$, and $LE_3 = 0.0000$ by selecting suitable values. Figure 6 shows the chaotic structure of the system with a positive Lyapunov exponent, illustrating its chaotic behavior. The approach of Lyapunov exponent iteration is presented in Table 1.

We use other methods, the strange attractor, the return map plots, the recurrence plot, and the power spectrum plot of the system (26), to detect whether chaos is present s for $w = 1, q = 1, a = 1, v = 2.6, u = 1.5, A = 1.736\ and\ \phi = 3.2$ with initial condition (0.11, 0.52). We demonstrate strange attractors for two state variables, P and Q, using the delay positions at 5 shown in Figs. 7 and 8. Then we see that the illustration's distinct paths behave chaotically and create a complex cyclic pattern.

The return map for the two-state variables, P and Q, is plotted in Fig. 9. The dispersed and non-repeating pattern illustrates the system's chaotic structure.

Figure 10 shows the recurrence plot for P and Q, two state variables, which determine the system behaves chaotically according to the irregular pattern of the graphics.

Figure 11 shows the power spectrum plot for two state variables, P and Q, which determine the system behaves chaotically according to the different frequency characteristics of the graphics.

Figure 12 shows the fractal dimension plot for the 0.9714 value, which is close to 1, indicating that the system behaves chaotically for Eq. (26).

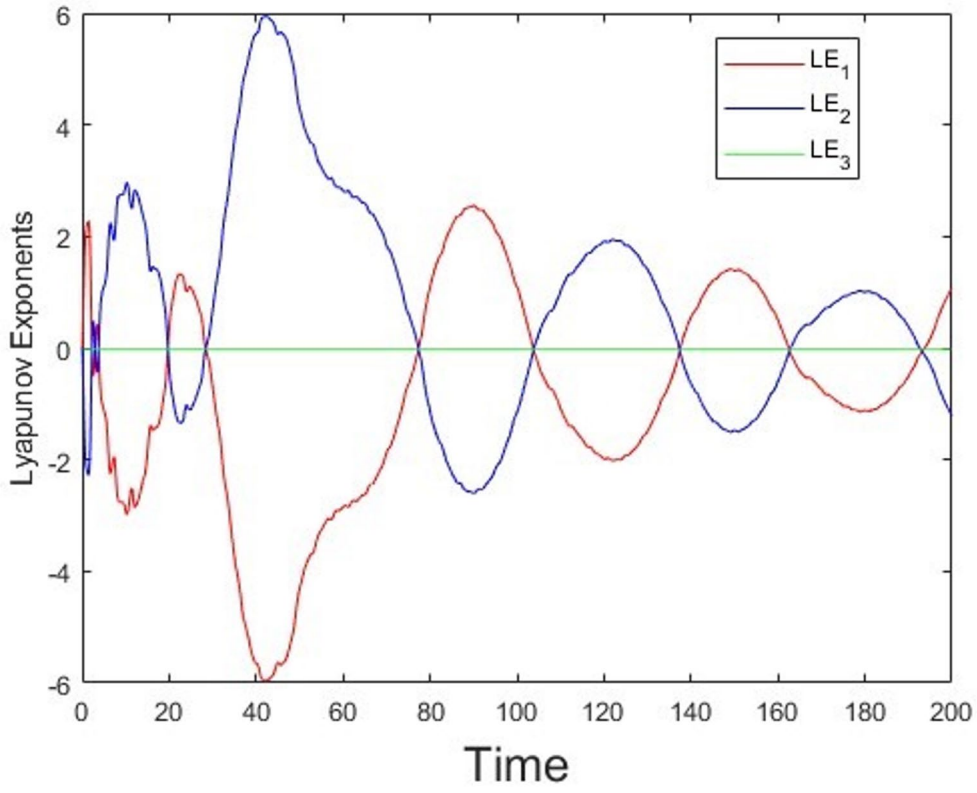


Fig. 6. Lyapunov exponent pattern of system Eq. (26) for $w = 1, q = 1, a = 1, v = 2.6, u = 1.5, A = 1.736\ and\ \phi = 3.2$ with initial value (0.11, 0.52).

Time	LE_1	LE_2	LE_3	Time	LE_1	LE_2	LE_3
10	−2.9269	2.9098	0.0000	110	−1.0778	1.0099	0.0000
20	0.32676	−0.34083	0.0000	120	−1.9893	1.9142	0.0000
30	−0.69296	0.67501	0.0000	130	−1.4924	1.4093	0.0000
40	−5.6494	5.6278	0.0000	140	0.55027	−0.63891	0.0000
50	−4.3142	4.2924	0.0000	150	1.3839	−1.4791	0.0000
60	−2.8503	2.8218	0.0000	160	0.49855	−0.6009	0.0000
70	−1.8735	1.8371	0.0000	170	−0.74649	0.63812	0.0000
80	1.0942	−1.1365	0.0000	180	−1.1181	1.0021	0.0000
90	2.5472	−2.5981	0.0000	190	−0.50856	0.38398	0.0000
100	1.0908	−1.1512	0.0000	200	1.0747	−1.2072	0.0000

Table 1. Iteration table for Lyapunov exponents.

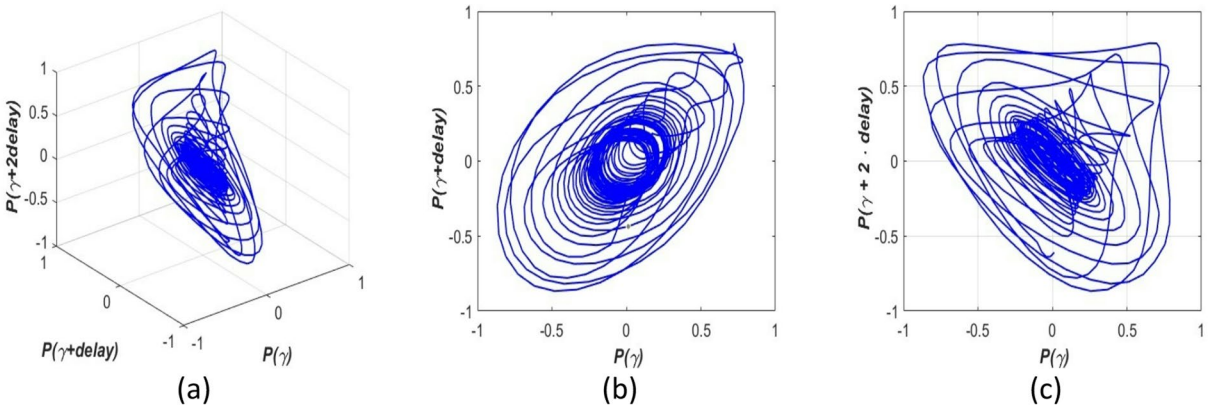


Fig. 7. Strange attractor for the state variable P of system for Eq. (26).

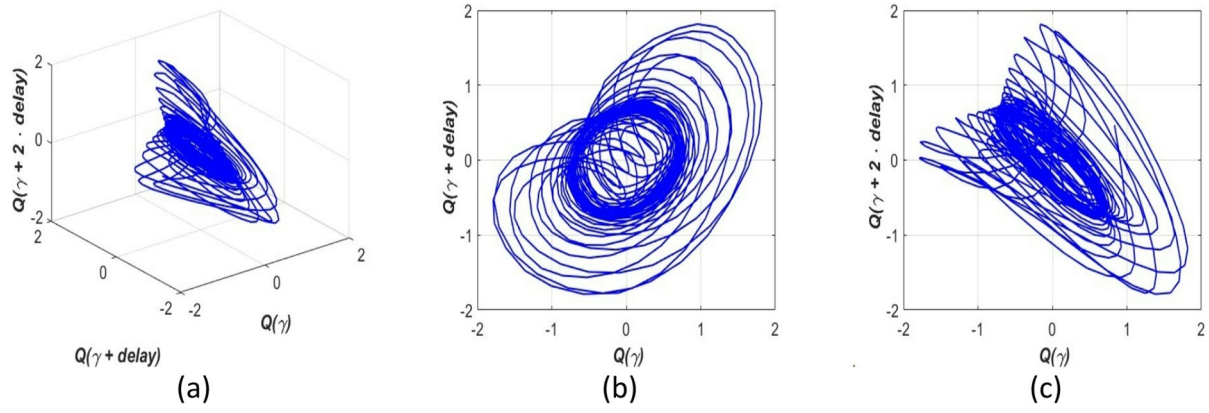


Fig. 8. Strange attractor for the state variable Q of system for Eq. (26).

Multistability analysis

The visualization of multi-stability[38,39] in the disturbed system controlled by Eq. (26) is found in this section. For finding the path of this dynamical system, the corresponding phase portraits are illustrated in Fig. 13. Multistability is an important characteristic that describe the existence of multiple stable points and the behavior of the path within a particular range of physical variables and initial conditions. For the initial values $(P(0), Q(0)) = (0.1, 0.1)$, $(P(0), Q(0)) = (-0.1,0.5)$, and $(P(0), Q(0)) = (0.3, -0.3)$, the colors red, blue, and green, respectively, can be used to create two different types of phase diagrams. Based on the given initial values, the system under analysis exhibits a chaotic pattern. The phase diagram shows that the existence of several stable states characterizes this chaotic behavior. Therefore, the system's multistability is complex and difficult to predict.

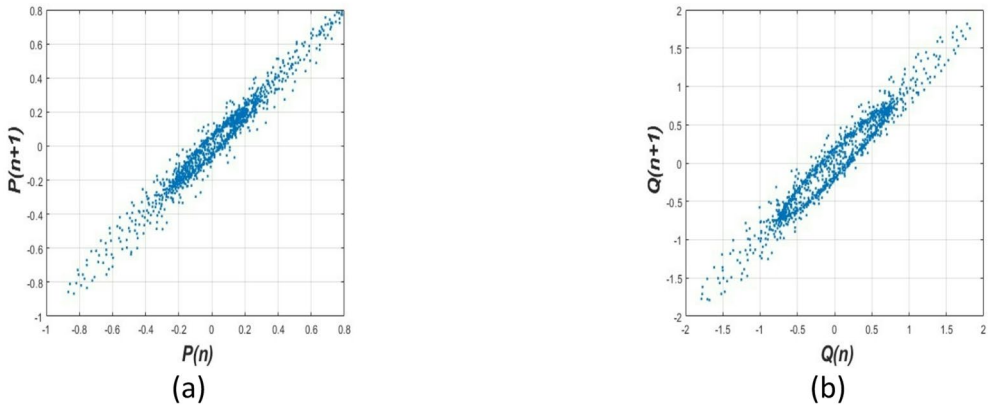


Fig. 9. Return map for state variable P and Q of system for Eq. (26).

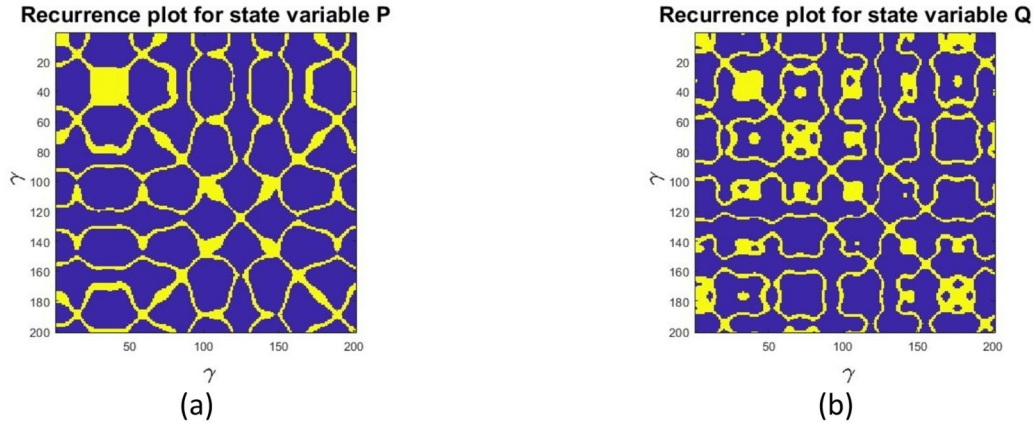


Fig. 10. Recurrence map for state variable P and Q of system for Eq. (26).

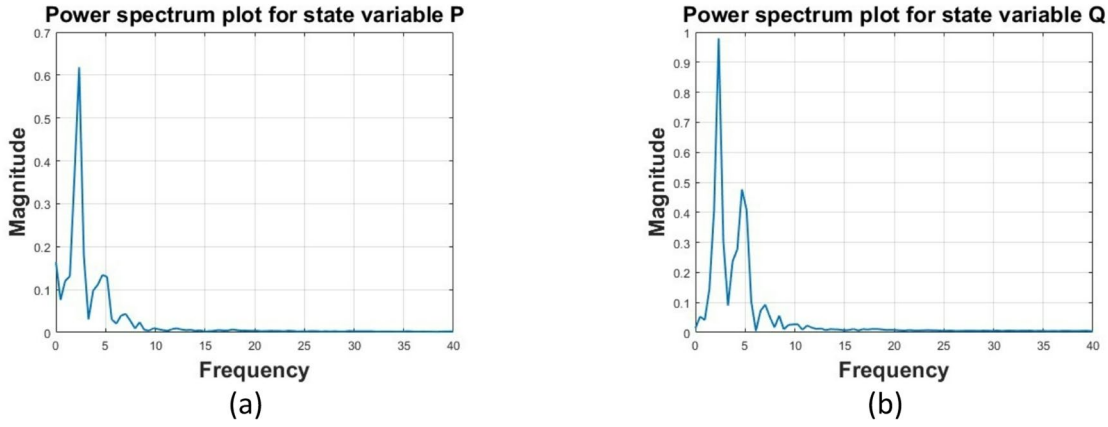


Fig. 11. Power spectrum plot for the state variable P and Q of the system for Eq. (26).

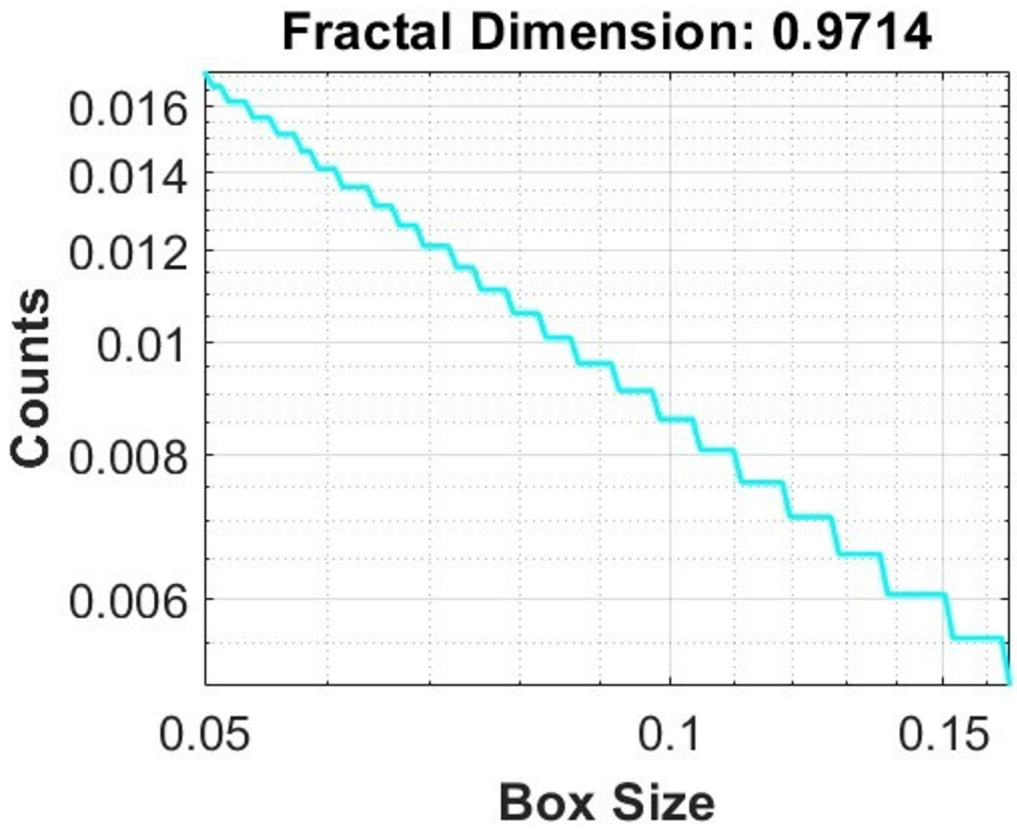


Fig. 12. Fractal dimension plot for Eq. (26).

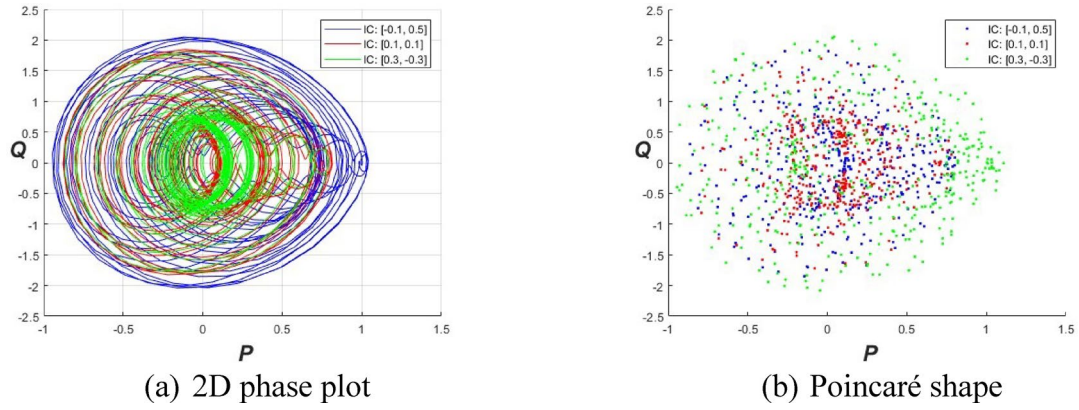


Fig. 13. Illustration of the system's multistability diagram of Eq. (26).

Uniqueness of our result

The work focuses on this study is different from others on the SRLW problem, as we find exact and numerous solutions, as well as visualize most of the possible behaviors of the solutions. This section compares our work with recent research and shows why our article is unique. Zhang and his colleagues[40] demonstrate bifurcation analysis and exact solutions to this model. ALA and his colleagues[41] are solving the SRLW equation using the IBSEFM method, and they find only three solutions. Hamali ana Alghamdi discovered exact solutions of the stated nonlinear problem supported by the Riccati-Bernoulli sub-ODE scheme[42]. Hussain and others obtain solitary waves of this model with the assistance of the tanh-coth method[43]. Aldwoah et al. extracted the analytical solutions of the mentioned equation through the φ^6 model expansion process[44]. However, we have obtained 18 solutions using the $\left(\frac{G\prime}{G^2}\right)$-expansion method, and all the illustrations are in 3D and 2D, and the insides are very advanced, likened to the above two papers. Additionally, various types of tools like power spectrum plots, recurrence plots, multi-stability diagrams, return maps, strange attractors, and Lyapunov exponents are

illustrated in this work to find the chaotic nature of the governing problem. We present the behavior of the solutions more clearly; we also present an analysis of their stability. Therefore, our investigation enhances the application capability of governing models in nonlinear research.

Future-oriented studies

Our work on the SRLW equation using chaotic nature, Lyapunov exponents, stability, multi-stability, and other chaos-detection techniques may open a wide range of research directions. After the current analysis has yielded useful information about the dynamic behavior of the equation, further research could focus on confirming these theoretical conclusions through practical experiments and numerical simulations.

Conclusion

We have successfully found new exact soliton solutions for the regularized long wave equation, utilizing the $\left(\frac{G\prime}{G^2}\right)$ -expansion method. Since this method is a mechanism for constructing precise soliton solutions, it is beneficial for solving nonlinear systems. We find the chaotic nature of the equation by using various types of tools like strange attractors, recurrence plots, return maps, Lyapunov exponents, power spectrum plots, and multi-stability analysis. The recurrence pattern helps us identify whether the equations are returning to similar conditions. A strange attractor gives us an idea about the equation's long-term behavior. Those analyses are important for finding chaotic behaviors in equations. These anticipated complicated dynamics and their real-world applications can be verified through physical experiments in the future based on our analysis and graphical description.

Data availability

All data generated or analysed during this study are included in this article.

Received: 16 October 2025; Accepted: 19 November 2025
Published online: 30 December 2025

References

1. Ullah, M. S., Roshid, H. O. & Ali, M. Z. New wave behaviors and stability analysis for the (2 + 1)-dimensional Zoomeron model. *Opt. Quant. Electron.* **56**, 240 (2024).
2. Ullah, M. S., Ali, M. Z. & Roshid, H. O. Stability analysis, φ^6 model expansion method, and diverse chaos-detecting tools for the DSKP model. *Sci. Rep.* **15**, 13658 (2025).
3. Ullah, M. S., Roshid, H. O. & Ali, M. Z. New wave behaviors of the Fokas-Lenells model using three integration techniques. *Plos One* **18**(9), 1–23 (2023).
4. Iqbal, M., Seadawy, A. R. & Lu, D. Construction of solitary wave solutions to the nonlinear modified Korteweg-de Vries dynamical equation in unmagnetized plasma via mathematical methods. *Mod. Phys. Lett. A*. **33** (32), 1850183 (2018).
5. Abdalla, M., Roshid, M. M., Ullah, M. S. & Hossain, I. Dynamical analysis, and the effect of fractional parameters on optical soliton solution for Yajima–Oikawa model in short-wave and long-wave. *Chaos Solitons Fract.* **199** (1), 116697 (2025).
6. Roshid, M. M. & Bashar, H. Breather wave and kinky periodic wave solutions of one dimensional Oskolkov equation. *Math. Model. Eng. Probl.* **6** (3), 460–466 (2019).
7. Serbay, D. Analysis of physical processes of the Kudryashov-Sinelshchikov equation with variable coefficients. *Int. J. Theor. Phys.* **64**, 139 (2025).
8. Iqbal, M., Seadawy, A. R., Lu, D. & Zhang, Z. Physical structure and multiple solitary wave solutions for the nonlinear Jaulent–Miodek hierarchy equation. *Mod. Phys. Lett. B*. **38** (16), 2341016 (2024).
9. Hossain, M. M., Abdeljabbar, A., Roshid, H. O., Roshid, M. M. & Sheikh, A. N. Abundant bounded and unbounded solitary, periodic, rogue-type wave solutions and analysis of parametric effect on the solutions to nonlinear Klein–Gordon model. *Complexity* 8771583 (2022).
10. Wang, K. J., Wang, G. D. & Shi, F. Diverse optical solitons to the Radhakrishnan–Kundu– Lakshmanan equation for the light pulses. *J. Nonlin Opt. Phys. Mater.* **33** (06), 2350074 (2024).
11. Usman, M., Hussain, A., Ali, H., Zaman, F. & Abbas, N. Dispersive modified Benjamin-Bona-Mahony and Kudryashov-Sinelshchikov equations: non-topological, topological, and rogue wave solitons. *Int. J. Math. Comput. Eng.* **3** (1), 21–34 (2025).
12. Attia, M., Attia, R. & Khater, M. M. A. The mBBM equation: a mathematical key to unlocking wave behavior in fluids. *Int. J. Math. Comput. Eng.* **3** (2), 171–184 (2024).
13. Inan, I. E., Duran, S. & Uğurlu, Y. TAN(F(ξ²))-expansion method for traveling wave solutions of AKNS and Burgers-like equations. *Optik* **138**, 15–20 (2017).
14. Duran, S., Durur, H. & Yokuş, A. Traveling wave and general form solutions for the coupled higgs system. *Math. Methods Appl. Sci.* **46**, 8915–8933 (2023).
15. El-Rashidy, K. New traveling wave solutions for the higher Sharma-Tasso-Olver equation by using extension exponential rational function method. *Results Phys.* **17**, 103066 (2020).
16. Usman, T., Hossain, I., Ullah, M. S. & Hasan, M. M. Soliton, multistability, and chaotic dynamics of the higher-order nonlinear Schrödinger equation. *Chaos* **35** (4), 043141 (2025).
17. Alqahtani1, A. M., Sharma, S., Chaudhary, A. & Sharma, A. Application of Caputo-Fabrizio derivative in circuit realization. *AIMS Math.* **10** (2), 2415–2443 (2025).
18. Jumarie, G. Modified Riemann–Liouville derivative and fractional Taylor series of nondifferentiable functions further results. *Comput. Math. Appl.* **51**, 1367–1376 (2006).
19. Wang, K. J. New exact solutions of the local fractional modified equal width-burgers equation on the cantor sets. *Fractals* **31** (09), 2350111 (2023).
20. Hossain, M. M., Roshid, M. M., Sheikh, M. A. N., Taher, M. A. & Roshid, H. O. Novel exact soliton solutions of Cahn–Allen models with truncated M-fractional derivative. *Int. J. Theor. Appl. Math.* **8** (6), 112–120 (2022).
21. Mostafa, M. & Ullah, M. S. Soliton outcomes and dynamical properties of the fractional Phi-4 equation. *AIP Adv.* **15**, 015105 (2025).
22. Khalil, R., Al Horani, M., Yousef, A. & Sababheh, M. A new definition of fractional derivative. *J. Comput. Appl. Math.* **264**, 65–70 (2014).
23. Abdeljawad, T. On conformable fractional calculus. *J. Comput. Appl. Math.* **279**, 57–66 (2015).

24. Serbay, D., Asıf, Y. & Gulsen, K. A study on solitary wave solutions for the Zoomeron equation supported by two-dimensional dynamics. *Phys. Scr.* **98**, 125265 (2023).
25. Atangana, D., Baleanu, A. & Alsaedi, A. New properties of conformable derivative. *Open. Math.* **13**, 1–10 (2015).
26. Serbay, D. An investigation of the physical dynamics of a traveling wave solution called a bright soliton. *Phys. Scr.* **96**, 125251 (2021).
27. Serbay, D. Dynamic interaction of behaviors of time-fractional shallow water wave equation system. *Mod. Phys. Lett. B.* **35**, 2150353 (2021).
28. Ali, K. K., Nuruddeen, R. I. & Raslan, K. R. New structures for the space-time fractional simplified MCH and SRLW equations. *Chaos Solitons Fract.* **106**, 304–309 (2018).
29. Korkmaz, A. & Hosseini, K. Exact solutions of a nonlinear conformable time fractional parabolic equation with exponential nonlinearity using reliable methods. *Opt. Quan Electron.* **49**, 278 (2017).
30. Silva, F. S., Davidson, M. M. & Marcelo, A. M. Conformable Laplace transform of fractional differential equations. *Axioms* **7**, 55 (2018).
31. Chen, J. P. & Chen, H. The $\left(\frac{G\prime}{G^2}\right)$-expansion method and its application to coupled nonlinear Klein–Gordon equation. *J. South. China Norm Univ.* **44**, 63–66 (2012).
32. Kang, Z. $\left(\frac{G\prime}{G^2}\right)$-expansion solutions to MBBM and OBBM equations. *J. Part. Diff Equ.* **28**, 158–166 (2015).
33. Alam, N., Ma, W. X., Ullah, M. S., Seadawy, A. R. & Akter, M. Exploration of soliton structures in the Hirota–Maccari system with stability analysis. *Mod. Phys. Lett. B.* **38**, 2450481 (2024).
34. Akter, M., Ullah, M. S., Wazwaz, A. M. & Seadawy, A. R. Unveiling Hirota–Maccari model dynamics via diverse elegant methods. *Opt. Quant. Electron.* **56**, 1127 (2024).
35. Sprott, J. C. A proposed standard for the publication of new chaotic systems. *Int. J. Bifur Chaos.* **21**, 2391–2394 (2011).
36. Jhangeer, A., Jamal, T., Talafha, A. M. & Riaz, M. B. Exploring travelling wave solutions, bifurcation, chaos, and sensitivity analysis in the (3+1)-dimensional gKdV–ZK model: a comprehensive study using lie symmetry methodology. *Results Eng.* **22**, 102194 (2024).
37. Han, T., Zhao, Z., Zhang, K. & Tang, C. Chaotic behavior and solitary wave solutions of stochastic-fractional Drinfel'd–Sokolov–Wilson equations with brownian motion. *Results Phys.* **51**, 106657 (2023).
38. Ganie, A. H., Rahaman, M. S., Aladsani, F. A. & Ullah, M. S. Bifurcation, chaos, and soliton analysis of the Manakov equation. *Nonlinear Dyn.* **113**, 1–15 (2025).
39. Rahaman, M. S., Islam, M. N. & Ullah, M. S. Bifurcation, chaos, modulation instability, and soliton analysis of the Schrödinger equation with cubic nonlinearity. *Sci. Rep.* **15**, 11689 (2025).
40. Zhang, J., Zheng, Z., Meng, H. & Wang, Z. Bifurcation analysis and exact solutions of the conformable time-fractional symmetric regularized long wave equation. *Chaos Solitons Fract.* **190**, 115744 (2025).
41. Ala, V., Demirbilek, U. & Mamedov, K. R. An application of improved Bernoulli sub-equation function method to the nonlinear conformable time-fractional SRLW equation. *AIMS Math.* **5**, 3751–3761 (2020).
42. Hamali, W. & Alghamdi, A. A. Exact solutions to the fractional nonlinear phenomena in fluid dynamics via the Riccati-Bernoulli sub-ODE method. *AIMS Math* **9** (11), 31142–31162 (2024).
43. Hussain, A., Jhangeer, A., Abbas, N., Khanc, I. & Nisar, K. S. Solitary wave patterns and conservation laws of fourth-order nonlinear symmetric regularized long-wave equation arising in plasma. *Ain Shams Eng. J.* **12**, 3919–3930 (2021).
44. Aldwoah, K. et al. Analytical solutions of the time-fractional symmetric regularized long wave equation using the φ^6 model expansion method. *Sci. Rep.* **15**, 16232 (2025).

Author contributions

Mohammad Safi Ullah: Conceptualization, Supervision, Writing-review & editing. Md. Mehedi Hasan: Software, Methodology, Writing-Original draft. Md. Aman Mahbub: Formal analysis, Writing-review & editing. All authors have read and agreed to publish the manuscript.

Funding

The author(s) received no external funding for this study.

Declarations

Competing interests

The authors declare no competing interests.

Additional information

Correspondence and requests for materials should be addressed to M.A.M.

Reprints and permissions information is available at www.nature.com/reprints.

Publisher's note Springer Nature remains neutral with regard to jurisdictional claims in published maps and institutional affiliations.

Open Access This article is licensed under a Creative Commons Attribution-NonCommercial-NoDerivatives 4.0 International License, which permits any non-commercial use, sharing, distribution and reproduction in any medium or format, as long as you give appropriate credit to the original author(s) and the source, provide a link to the Creative Commons licence, and indicate if you modified the licensed material. You do not have permission under this licence to share adapted material derived from this article or parts of it. The images or other third party material in this article are included in the article's Creative Commons licence, unless indicated otherwise in a credit line to the material. If material is not included in the article's Creative Commons licence and your intended use is not permitted by statutory regulation or exceeds the permitted use, you will need to obtain permission directly from the copyright holder. To view a copy of this licence, visit http://creativecommons.org/licenses/by-nc-nd/4.0/.

© The Author(s) 2025